Automatic Digital Modulation Classification using Extreme Learning Machine with Local Binary Pattern Histogram Features

Ahmet Güner[a], Ömer Faruk Alçin[a,*], Abdulkadir Şengür[b]

[a] *Department of Electrical-Electronics Engineering, Bingöl University, 12000 Bingöl, Turkey*
[b] *Department of Electrical and Electronics Engineering, Fırat University, 23000 Elazıg, Turkey*

Abstract

Discrimination of the Local Binary Pattern (LBP) in the classification of different digital modulation types was investigated in this study. It has been shown that LBP can be used as a feature extraction method for AMC schemes. A new AMC scheme is proposed using Extreme Learning Machine (ELM) as a classifier, which has a faster learning process and better generalization performance than conventional machine learning methods. The study also investigated the stability of the proposed AMC scheme, which is affected by variation in the values of the roll-off factor, frequency and phase offset that can affect the stability and performance of the system. Through simulation, a classification accuracy of over 95% was achieved at low SNR levels such as -2 dB. It was also shown that the proposed AMC scheme is more successful under similar conditions when making comparisons to other studies.

Keywords: Automatic modulation classification, extreme learning machine, local binary pattern, digital modulation

1. Introduction

The Automatic Modulation Classification (AMC) was first used in the military field for the identification of transmitted signals. In recent years, in both military and commercial applications, the importance of AMC has increased further with the widespread adoption of intelligent receivers such as cognitive radio and soft defined radios, which can automatically adapt to communications standards [1].

The AMC is located prior to the demodulation process, which is the last operation of the process of obtaining information messages from the received signal. AMC becomes even more important in real communication scenarios where synchronization errors occur due to time offset, frequency offset and multipath fading effects.

The two main algorithms used to classify modulated signals are maximum likelihood and feature-based. With the maximum likelihood algorithm, the likelihood function is calculated for each modulation format, and the decision is made based on the maximum of this function [2].

The feature-based algorithm consists of two steps: the feature extraction of the received signal and the feature classification for determination of the modulation type. When previous research found in the literature is investigated, it can be seen that various feature extraction methods with classifiers are combined in different ways, so AMC schemes are determined. Two methods have been proposed by Nandi and Azzouz for the classification of analogue and digital modulation types [3]. The instantaneous amplitude, instantaneous phase and instantaneous frequency parameters of the received signals are used as features in both methods. In the first method, the decision tree approach was employed, which was developed in order to classify different types of modulation and contains a set of decision criteria. In the second method,

*Corresponding author
Email address: ofalcin@bingol.edu.tr (Ömer Faruk Alçin)

artificial neural networks were used in the modulation classification process. Swami and Sadler proposed a method in which the fourth-order cumulants were selected as features and the hierarchical decision tree structure used as the classifier for classifying M-QAM, M-PSK, and M-ASK modulation types [4], and is a reference study, especially for research that employs high-order cumulants as features. Wang Yu et al. presented a method using instantaneous amplitude, frequency, phase information of the signal, normalized fourth-order cumulants and wavelet detail as features, and used PSO-support vector machines as classifiers [5]. Mobasseri chose the constellation shape as a feature and then classified the selected modulation types with a Fuzzy-C means clustering method [6]. Wong and Nandi used artificial neural network (ANN) and genetic algorithm (GA) for modulation classification, and resilient back propagation algorithm for multi-layer perceptron recognizer. GA was used to select the best features from a combined spectral and statistical feature set [7]. Timothy OShea et al. used raw I/Q data combined with convolution neural network (CNN) to achieve promising results. However, certain effects such as I/Q balance and phase offset may affect the accuracy of AMC using raw I/Q data [8].

As outlined, various feature types have been used in AMC schemes, e.g., high-order statistics [4, 9], cyclostationarity [10, 11, 12], instantaneous parameters [3, 5, 13] and wavelet coefficients [13, 14]. The point here is that if the AMC schemes are designed carefully by choosing the proper set of features, near optimal results can be obtained.

In the current study, the 1-dimensional LBP (1-D LBP) method is proposed for AMC as a new feature extraction method. Local binary pattern (LBP) is a texture descriptor that has proven quite effective for various image analysis tasks including texture classification, face recognition and image retrieval applications [15, 16, 17]. Recently, the 1-D LBP version of LBP has been extensively used in signal processing applications [18, 19]. Chatlani successfully used 1-D LBP method to detect voice activity in speech signals [18].

Digital communication systems offer various challenges and opportunities for machine learning algorithms. Nowadays, machine learning is widely used in areas such as image processing [20, 21], signal processing [22] and power electronics [23]. Moreover, machine learning applications play an important role in AMC schemes. In the proposed AMC scheme, an extreme learning machine (ELM) is used as a classifier as shown in Figure 1. There are two important reasons for recommending 1-D LBP in feature extraction. The first is the simplicity of use, and the second is that the complexity of operation may be low due to its simplicity. The reason why ELM is preferred for the classifier is that it is faster than other classifiers and has advantages such as better generalization performance [24].

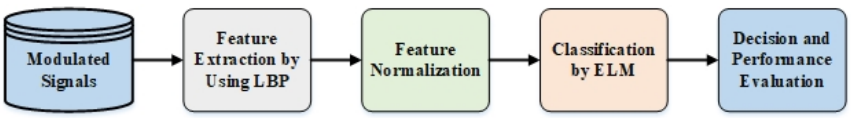

Figure 1: Block diagram of the proposed AMC scheme

In the current study, a new AMC scheme is proposed in order to determine the ASK, PSK and QAM modulation types within additive white Gaussian noise (AWGN) channels. These modulation types were preferred because ASK, PSK and QAM are widely used in both military and civil communications. When the proposed AMC scheme was tested, different modulation levels, unexpected phase, frequency and time offsets in wireless communication systems, noise, Doppler shift and pulse shape filter effects were considered.

The remainder of the paper is organized as follows. The signal model is explained in the second section. The third section provides information about the LBP and describes the use of the 1-D LBP as a feature in the classification of digital modulation types. The fourth section presents the structure of the extreme learning machine, and the fifth section presents the simulation results and their analysis.

2. Signal model

In wireless communication systems, a digitally modulated signal (y) is generally expressed as in (1).

$$y\left(t\right) = he^{j(2\pi\Delta ft+\theta+\varphi(t))}\sum_{k} s_k g(t - kT - t_0) + w\left(t\right) \tag{1}$$

Here, s is a complex-value, zero-mean, independent and identically distributed (i.i.d.) symbol sequence, which is drawn from an alphabet of symbols (the constellation) that defines the modulation scheme, where θ is the phase offset, T is the symbol rate, t_0 is the timing offset, Δf is the carrier frequency offset, $\varphi(t)$ is the phase noise and $w(t)$ additive white Gaussian noise with σ_w^2 variance. The factor $g(t)$ defines the shape of the pulse. In this signal model, a common example is the raised cosine frequency shaping filter with roll-off factor (β is the roll-off factor between 0 and 1). The imperfections in transmitter and receiver oscillators cause phase noise which is a result of carrier frequency fluctuation. Phase noise is generally modeled by a Wiener random process with zero mean and variance $2\pi B_L|t|$, where B_L represents the 3dB bandwidth of the Lorentzian power spectrum of the oscillators [25].

In the case of Doppler shift, Rayleigh fading channel coefficient is expressed [26] as in (2)

$$h_l = \sum_{i=1}^{N} Ae^{j(\alpha_i + \frac{2\pi V l T_s}{\lambda} Cos\theta_i)} \tag{2}$$

Here, N is the number of beams from different α_i angles to the receiver and α_i random changes between $(0, 2\pi)$, A is the coefficient of power delay profile of the mobile channel, λ is the wavelength of the carrier signal, T_s is the sampling period,l is the time index along the data packet, V is the velocity of the mobile transmitter or receiver and θ_i is the angle between the movement direction of the vehicle and the antenna.

Having become widespread in digital communication systems, the use of digital modulation schemes has also been increasing. In original digital communication systems, fixed order modulation such as BPSK, QPSK, and 8PSK is the most widely adopted system.

For this reason, the proposed AMC scheme aimed to classify BPSK, QPSK, 8-PSK, 16-QAM, 64-QAM and 4-ASK linear modulation types.

3. Local binary pattern

LBP is an effective and productive method for image processing applications. Using LBP, locally repeating patterns are revealed. LBP is usually applied to 3x3 pixel images. In the LBP, the central value of the 3x3 pixel images is re-encoded with respect to the neighboring eight pixels. An illustrative visual example of the LBP method is shown in Figure 2.

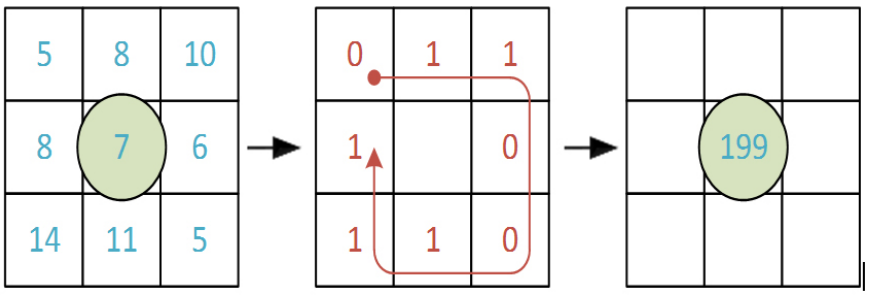

Figure 2: LBP coding for 3x3 pixel image

When LBP encoding is performed, grey level values are considered. The central pixel value is compared with the first pixel (left-top) value. If the central pixel value is greater than the first pixel value, it is encoded

as 1, else it is encoded as 0. This is performed for other neighboring pixels as well. The binary number is encoded starting from the left-top pixel, and after proceeding in the direction shown in Figure 2, an 8-bit binary number is obtained. The new value of the center pixel is the decimal equivalent of the 8-bit binary number obtained [27].

P_1	P_2	P_3	P_4	P_c	P_6	P_7	P_8	P_9

Figure 3: 1-D LBP window structure

3.1. 1-D local binary pattern

In the 1-D LBP conversion process from LBP, nine sample-length window structures are considered instead of the 3x3 pixel image. This window structure is shown in Figure 3.

In Figure 3, P_i represents the i^{th} sample in the window, and P_c represents the fifth sample, which is termed as the central sample. The basic mathematical expression of the 1-D LBP method is presented in Equation 3.

$$P_c = \sum_{i=1}^{N} f\,(x) 2^{i-1} \tag{3}$$

Here, $f(x)$ is the sign function

$$f(x) = \begin{cases} 0, P_i > P_c \\ 1, P_i < P_c \end{cases} \tag{4}$$

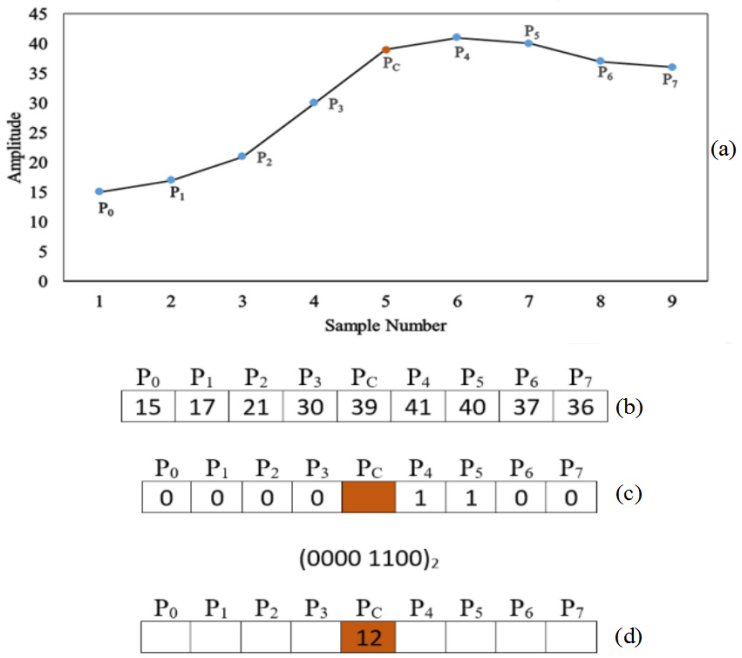

Figure 4: 1-D LBP encoding for a sample signal

In order to illustrate this operation, let us consider a signal such as x (x = 15, 17, 21, 30, 39, 41, 40, 37, 36) as shown in Figure 4a and 4b. In the 1-D LBP, an 8-bit binary sequence is obtained, starting from the leftmost neighbor (P_1) and comparing the neighboring sequences to the central sample, as shown in Figure 4c. The central sample value is obtained by converting the 8-bit binary number to decimal, using Equation 3 (see Figure 4d). The 1-D LBP process is performed by sliding the window along the entire signal [19].

3.2. Feature extraction with local binary pattern

In this study, 1-D LBP method was used for extracting features from the digital modulated signals. QAM, ASK and PSK modulated signals vary in amplitude and phase information according to the shape of the constellation diagram. This change affects the real and imaginary parts of the complex signal. Here, the effect of both parts on performance is taken into account.

After the signal vectors of the real and imaginary parts of the modulated signal are evaluated separately, the feature vector is formed by combining the features extracted from the signal vectors. For all samples (see Figure 5a) of the signal vector, a 1-D LBP signal with values in the range of 0 to 255 (see Figure 5b) is obtained by applying the procedure described in Figure 4. Each 1-D LBP sample value corresponds to a different pattern. The histogram of the 1-D LBP signal (see Figure 5c) shows the frequency of these various patterns.

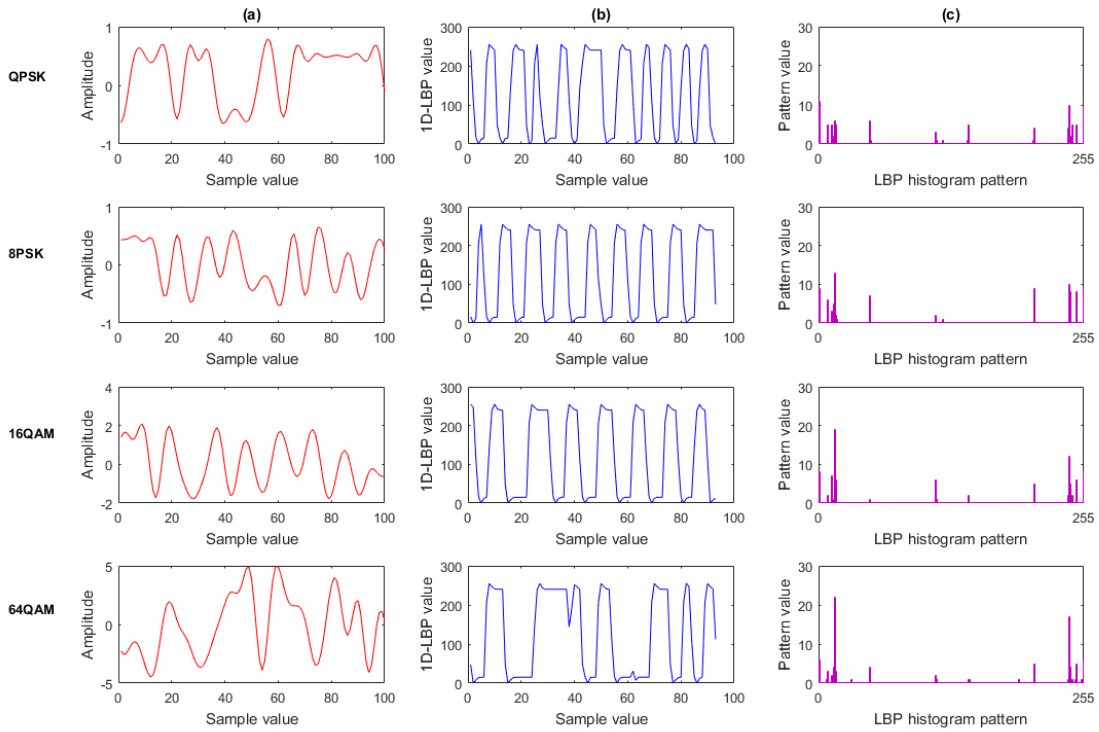

Figure 5: 1-D LBP applied signal with root raised cosine pulse shaping and roll offfactor equals 0.25 for QPSK, 8-PSK, 16-QAM and 64-QAM modulation format. (a) Modulated signal without noise (b) LBP applied signal (c) LBP histogram

With the increase of modulation level, intermediary levels are formed and it was observed that the number of instantaneous changes in the rises ($P = \{0,0,0,0,1,1,1,1\}_2 = 15_{10}$) and in drops ($P = \{1,1,1,1,0,0,0,0\}_2 = 240_{10}$) are decreased. This led to a reduction in the number of various patterns and an increase in the number of different pattern frequencies. Figure 5c shows histograms of 1-D LBP

signals with different modulation levels. Here, it is clear from the changes seen in Figure 5c that the intensity in the central regions shifts towards the right and left regions with increasing modulation level, and also that there are increases in the number of pattern frequencies corresponding to the rises and drops. For these reasons, 1-D LBP has a distinctive feature characteristic for the classification of M-QAM, M-ASK and M-PSK digital modulation types.

4. Extreme learning machine (ELM)

ELM is a recommended learning algorithm for the Single Hidden Layer Feedforward (SLFN) neural network [28, 29, 24]. ELM input weights and hidden layer threshold values are randomly generated and remain constant throughout the process, unlike conventional feed-forward networks. The output weights of the ELM are calculated analytically. With this approach, the rapid learning process is realized. In addition, ELM exhibits better generalization performance when compared to conventional feed-forward networks [30]. The SLFN network model is illustrated as in Figure 6.

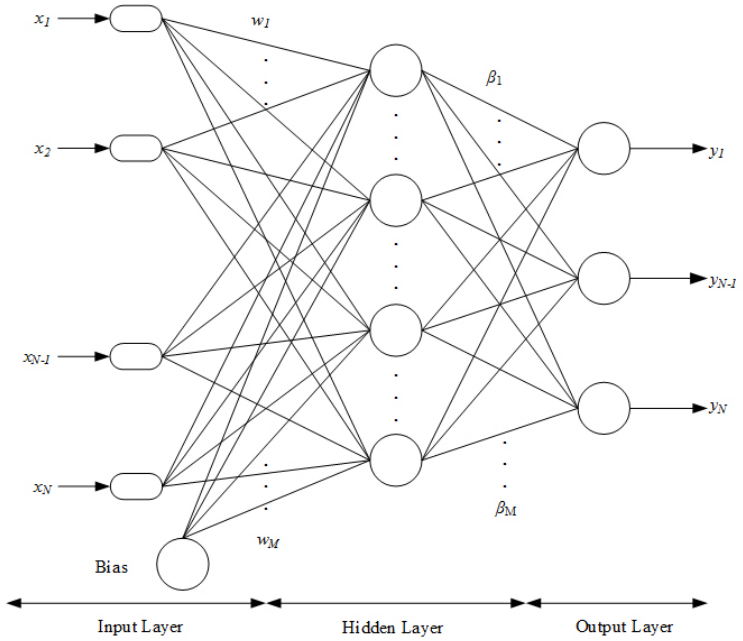

Figure 6: SLFN network architecture

For the SLFN network given in Figure 6, it is assumed that there is an input-output ($x_i = [x_{i1}, x_{i2}, \ldots, x_{in}]^T$,$y_i = [y_{i1}, y_{i2}, \ldots, y_{in}]^T$) pair possessing N samples. This input-output pair and the mathematical model of the SLFN network with M number of hidden layer neuron and $g(x)$ activation function can be given as;

$$\sum_{i=1}^{M} \beta_i g\left(w_i.x_j + b_i\right) = o_j, j = 1, \ldots, N \tag{5}$$

Where $w_i = [w_{i1}, w_{i2}, \ldots, w_{in}]^T$ is the input weight vector, $\beta_i = [\beta_{i1}, \beta_{i2}, \ldots, \beta_{im}]^T$ is the output layer weight vector, b_i is the threshold value of the i^{th} hidden neuron, and $o_j = [o_i, o_i, \ldots, o_j]^T$ is the output of the SLFN network. In Equation 5, $(w_i.x_j)$ is the scalar product of w_i and x_j. If the SLFN network is assumed to $\sum_j \|o_j - y_j\| = 0$, the model can be written as;

$$\sum_{i=1}^{M} \beta_i g\left(w_i.x_j + b_i\right) = y_j, j = 1, \ldots, N \tag{6}$$

The N equations given here can be expressed in matrix form as;

$$Y = H\beta \tag{7}$$

Where H is the hidden layer output matrix, β is the output layer weights, and Y is the output vector. H, β and Y expressions are given in Equation 8.

$$H = \begin{bmatrix} g\left(w_1 x_1 + b_1\right) & \cdots & g\left(w_N x_1 + b_N\right) \\ \vdots & \ldots & \vdots \\ g\left(w_1 x_M + b_1\right) & \cdots & g\left(w_N x_M + b_N\right) \end{bmatrix}_{NxM} \quad \beta = \begin{bmatrix} \beta_1^T \\ \vdots \\ \beta_M^T \end{bmatrix}_{Mx1} \quad Y = \begin{bmatrix} y_1^T \\ \vdots \\ y_N^T \end{bmatrix}_{Nx1} \tag{8}$$

As can be seen from Equation 6, the SLFN network can be expressed by a linear equation. In ELM, training of the network is carried out through the calculation of β. This can be shown as;

$$\beta = H^{\dagger} Y \tag{9}$$

Here, $H^{\dagger}$, indicates the Moore Penrose generalized reverse of H [28, 29, 24].

Table 1: Signal parameters

Parameter	Value
Carrier frequency	$f_c = 10$ MHz
Sampling rate	$f_s = 1.12$ MHz
Symbol rate	$1/T_s = 280$ KHz
Number of symbol	$N = 2048$

5. Simulation results and evaluations

Six of the most popular modulations were selected to form a candidate modulation type. These were BPSK, QPSK, 8-PSK, 16-QAM, 64-QAM and 4-ASK. The alphabet set from the symbol mapping for each modulation was normalized to zero mean and unit power in MATLAB. When simulating the transmitted signal symbols, each symbol was assigned from the alphabet set with equal probability. Then, for each modulation type, a dataset consisting of 1,000 signals and a total of 6,000 signals was generated by using the parameter values given in Table 1. In order to test the performance of the proposed automatic modulation classifier, the dataset was prepared by adding AWGN noise with SNR levels between -10 dB and 10 dB, with a 1 dB increase. In order to demonstrate the validity of the proposed AMC scheme, 10-fold cross-validation was used.

The ELM parameters for the current study were obtained through an empirical approach, with the number of hidden neuron as 220 and the activation function was *sigmoid*.

Channel parameters such as channel gain, noise variance, carrier phase offset and carrier frequency offset were considered the most important in the classification decision [1].

In the simulations performed, the performance analyses of the proposed AMC scheme were conducted against conditions in the receiver such as the frequency, phase and timing offset, symbol number, the roll-off parameter value of the raised cosine filter, phase noise, impulsive noise and Doppler shift.

First, known channel scenarios were applied for the accuracy analysis of the proposed AMC scheme. In other words, it was assumed that the phase offset and frequency offset effects were compensated prior to the modulation classifier. When the results shown in Figure 7 and Table 2 are analyzed, it can be seen that the proposed AMC scheme has high classification accuracy.

In the reference [1] prepared by Zhu and Nandi, BPSK, QPSK, and 4-ASK were shown to have higher classification accuracy at the low SNR levels. However, as the modulation level increased, such as with 16-QAM and 64-QAM, the SNR value required for classification also increased. In addition, in [1], 64-QAM was shown to have higher classification accuracy than 16-QAM in comparisons using different AMC schemes. As shown in Figure 7, 64-QAM was shown to have higher classification accuracy than either QPSK or 16-QAM. The reason for this is that the distinctive feature of the LBP histogram distribution is enhanced by the increasing level of modulation (see Figure 5c). One-dimensional modulation types such as BPSK and 4-ASK have higher classification accuracy at low SNR levels than modulation types on two dimensions such as QPSK, 8-PSK and 16-QAM. This is because the signal vectors of the real and imaginary parts of the modulated signal are separately evaluated and then the feature vector is merged with the features extracted from the signal vectors of the real and imaginary parts.

For the robustness of the proposed AMC scheme, its performance at different SNR levels was investigated according to the changes in the symbol number, phase offset, frequency offset and roll-off parameter of the raised cosine filter, which is the impulse shaping filter.

As can be seen in Figure 8, the performance of the proposed AMC scheme was significantly affected by the variation of the symbol number. Here, with the increase in the symbol number, the increase in the classifier performance is an indication of the consistent operation of the proposed AMC structure. When the SNR level was greater than -2 dB, the average classification accuracy was $> 95\%$ for all modulations. The symbol number required was 2048 in order that the classification accuracy could be higher at low SNR levels.

In Figure 8, the effect of the number of symbols was analyzed using a fixed window of the received samples, because the effect of the sampling rate is similar to the effect of the number of symbols. That is, increasing the sampling rate means fewer symbols are packed into the fixed window. Therefore, the curves seen in Figure 8 show the increase in the sampling rate leading to a decrease in the classifier performance. In other words, higher classifier performance is obtained at low sampling rates.

The AMC scheme in [4] provides good performance in classifying selected modulation types, but does not allow for clear distinguishing between 16-QAM and 64-QAM types. In the same way, the same problem was encountered in the AMC scheme proposed by [7]. The AMC scheme proposed in [31] was composed of two stages. In the first stage, the 16-QAM and 64-QAM types were evaluated as a whole within a group while separating the selected modulation types. In the second stage, only 16-QAM and 64-QAM types were distinguished. In this way, the separation performance between 16-QAM and 64-QAM increases. As can be understood from this, 16-QAM separation from 64-QAM is important because QAM is widely used in many communication systems for all types of modulation.

Figure 9 shows the performance variation of the proposed AMC scheme between 16-QAM and 64-QAM. In comparison with other references, in [32],Dobre, Ness, and Su used cyclic cumulants in the 16-QAM and 64-QAM classifications and obtained 70% classification accuracy at SNR = 10 dB. In [31], Aslam, Zhu, and Nandi obtained 99.4% classification accuracy at the same SNR value; and in [4], Swami and Sadler obtained 90% classification accuracy at SNR = 15 dB. In the proposed AMC scheme of the current study, 95.1% classification accuracy was achieved at SNR = 0 dB.

As can be seen in Figure 10, the phase offset has a small effect on the classifier performance at SNR levels lower than -1 dB, but has almost no significant effect at SNR $\geq$ -1 dB levels.

As can be seen in Figure 11, the frequency offset has an effect on the classifier performance at low SNR levels. However, for $\Delta f < \%6 f_c$ at a level of SNR $\geq$ 1 dB, there was a significant decrease in the effect rate. The proposed AMC scheme was hardly affected by the phase offset, but was affected only slightly where the frequency offset had high values. The reasons for this are that, when QAM modulated signals are compared with PSK modulated signals, the classification of 16-QAM and 64-QAM types is less sensitive to frequency offsets and requires high SNR for a high degree of accuracy.

Typical roll-off (β) values for wireless communication systems range from 0.2 to 0.4 [33]. As can be seen in Figure 12, the proposed AMC scheme is similar to the specified roll-off range and showed the best performance. However, in the case of $\beta > 0.4$, a small decrease in classifier performance was seen between SNR value of -2 dB and 6 dB. In the case of SNR $\geq$ 6 dB, the change of the roll-off value negligibly affects classifier performance.

In conventional communication systems, there are three noise sources, which are additive white Gaussian noise, phase noise from transmitter and receiver oscillators, and impulsive noise from various natural and manmade sources.

The effect of phase noise on the performance of the proposed AMC scheme was as shown to be negligible (see Figure 13) and therefore robust against the presence of phase noise.

An impulsive noise consists of short duration pulses of random amplitude, duration, and time of occurrence. There are many reasons for the generation of impulsive noises, including electromagnetic interferences and defects and faults in communication and transmission systems. An impulsive noise may be modeled as the output of a filter excited by an amplitude-modulated random binary sequence [34].

Figure 14 illustrates a digitally modulated signal with AWGN (SNR = 10 dB) and impulsive noise (IN) with 10% impulse.

BER versus signal to noise ratio (SNR) performances of the proposed AMC scheme for AWGN and AWGN with impulsive noise are illustrated as shown in Figure 15. It is seen that at a level of SNR > -4 dB, the proposed AMC scheme was affected by the impulsive noise. The reason for this is that in the intermediary levels of the 1-D LBP applied signal histogram (see Figure 5c), impulses with random amplitude and occurrence time in the impulsive noise caused an increase in the number of different patterns. This led to a reduction in the performance of the proposed AMC scheme. However, it is clear that as the amplitude and number of impulses increases, the performance of the proposed AMC scheme decreases.

Figure 16 shows how a single channel coefficient varies with the effect of Doppler shift according to the different velocities of the mobile device during the transmission of a data packet. When the packet length is the same, the increase in the velocity of the mobile device causes a variation in the channel coefficient values from the beginning to the end of the packet. When there is no Doppler shift, it is assumed that the channel coefficients do not change during data packet transmission.

As can be seen in Figure 17, the performance of the proposed AMC scheme was significantly affected by the Doppler shift, due to its high velocity. Here, with the increase in velocity, the variation seen in the classifier performance is an indication that the proposed AMC structure is not consistent under the effect of Doppler shift.

The effect of timing offset on the performance of the proposed AMC scheme can be seen in Figure 18, in which the proposed AMC scheme was shown to be robust against the presence of timing offset.

Table 3 shows a comparison of the proposed AMC scheme to the reference works found in the literature. When Table 3 is examined, it can be seen that the proposed AMC scheme has higher performance at low SNR levels than the other methods in determining modulation types widely used in digital communication.

6. Conclusion

Due to the widespread application of digital communications in wired, wireless and optical communication systems, and the increased usage of digital signal processing methods on the receiver side, the estimation of signal parameters has now become more significant. The feasible and fast determination of the modulation type against the signal parameters is the intended purpose; therefore, a new AMC scheme has been presented in this paper which tested as having high classification accuracy at low SNR levels, and robustness against different situations that can occur in the receiver. The simplicity, feasibility and performance of the proposed method has been demonstrated through simulated results and comparisons to the literature. The study presents that the LBP, which is used as a feature in numerous different areas, can also be used as a feature in the classification of digital modulation types.

In future works, multi-carrier digital modulations will be classified with recent deep learning methods.

[1] Z. Zhu, A. K. Nandi, Automatic Modulation Classification: Principles, Algorithms and Applications, 1st ed. ed., Wiley Publishing, 2015. doi:10.1002/9781118906507. arXiv:arXiv:1011.1669v3.

[2] F. Hameed, O. A. Dobre, D. C. Popescu, On the likelihood-based approach to modulation classification, IEEE Transactions on Wireless Communications 8 (2009) 5884–5892. doi:10.1109/TWC.2009.12.080883.

[3] A. K. Nandi, E. E. Azzouz, Algorithms for automatic modulation recognition of communication signals, IEEE Transactions on Communications 46 (1998) 431–436. doi:10.1109/26.664294.

[4] A. Swami, B. Sadler, Hierarchical digital modulation classification using cumulants, IEEE Transactions on Communications 48 (2000) 416–429. doi:10.1109/26.837045.

[5] Y. Wang, T. Zhang, J. Bai, R. Bao, Modulation recognition algorithms for communication signals based on particle swarm optimization and support vector machines, in: 2011 Seventh International Conference on Intelligent Information Hiding and Multimedia Signal Processing, 2011, pp. 266–269. doi:10.1109/IIHMSP.2011.31.

[6] B. G. Mobasseri, Digital modulation classification using constellation shape, Signal Processing 80 (2000) 251–277. doi:10.1016/S0165-1684(99)00127-9.

[7] M. Wong, A. Nandi, Automatic digital modulation recognition using artificial neural network and genetic algorithm, Signal Processing 84 (2004) 351–365. doi:10.1016/j.sigpro.2003.10.019.

[8] T. J. O'Shea, J. Corgan, T. C. Clancy, Convolutional radio modulation recognition networks, in: C. Jayne, L. Iliadis (Eds.), Engineering Applications of Neural Networks, 2016, pp. 213–226. doi:10.1007/978-3-319-44188-7_16. arXiv:1602.04105.

[9] D. Chang, P. Shih, Cumulants-based modulation classification technique in multipath fading channels, IET Communications 9 (2015) 828–835. doi:10.1049/iet-com.2014.0773.

[10] H. Wang, L. Guo, A new method of automatic modulation recognition based on dimension reduction, in: Forum on Cooperative Positioning and Service (CPGPS), 2017, pp. 316–320. doi:10.1109/CPGPS.2017.8075146.

[11] Q. Zhang, O. A. Dobre, Y. A. Eldemerdash, S. Rajan, R. Inkol, Second-order cyclostationarity of BT-SCLD signals: Theoretical developments and applications to signal classification and blind parameter estimation, IEEE Transactions on Wireless Communications 12 (2013) 1501–1511. doi:10.1109/TWC.2013.021213.111888.

[12] O. A. Dobre, Signal identification for emerging intelligent radios: classical problems and new challenges, IEEE Instrumentation Measurement Magazine 18 (2015) 11–18. doi:10.1109/MIM.2015.7066677.

[13] A. Hazza, M. Shoaib, S. A. Alshebeili, A. Fahad, An overview of feature-based methods for digital modulation classification, in: 1st International Conference on Communications, Signal Processing and Their Applications, ICCSPA, 2013, pp. 1–6. doi:10.1109/ICCSPA.2013.6487244.

[14] W. Hamouda, K. Hassan, I. Dayoub, M. Berbineau, Automatic modulation recognition using wavelet transform and neural networks in wireless systems, Eurasip Journal on Advances in Signal Processing (2010). doi:10.1155/2010/532898.

[15] M. Pietikäinen, Image analysis with local binary patterns, in: H. Kalviainen, J. Parkkinen, A. Kaarna (Eds.), Image Analysis, 2005, pp. 115–118. doi:https://doi.org/10.1007/11499145_1.

[16] A. Hadid, G. Zhao, T. Ahonen, M. Pietikäinen, Face Analysis Using Local Binary Patterns, Imperial College Press, 2008.

[17] T. Ahonen, A. Hadid, M. Pietikäinen, Face recognition with local binary patterns, in: European Conference on Computer Vision, 2004, pp. 469–481. doi:10.1007/978-3-540-24670-1_36.

[18] N. Chatlani, J. J. Soraghan, Local Binary Patterns for 1-D Signal Processing, in: 18Th European Signal Processing Conference (Eusipco), volume 18, 2010, pp. 95–99.

[19] P. McCool, N. Chatlani, L. Petropoulakis, J. J. Soraghan, R. Menon, H. Lakany, Lower arm electromyography (EMG) activity detection using local binary patterns, IEEE Transactions on Neural Systems and Rehabilitation Engineering 22 (2014) 1003–1012. doi:10.1109/TNSRE.2014.2320362.

[20] M. Cibuk, U. Budak, Y. Guo, M. C. Ince, A. Sengur, Efficient deep features selections and classification for flower species recognition, Measurement 137 (2019) 7 – 13. URL: http://www.sciencedirect.com/science/article/pii/S0263224119300284. doi:https://doi.org/10.1016/j.measurement.2019.01.041.

[21] M. Aslan, A. Sengur, Y. Xiao, H. Wang, M. C. Ince, X. Ma, Shape feature encoding via fisher vector for efficient fall detection in depth-videos, Applied Soft Computing 37 (2015) 1023 – 1028. URL: http://www.sciencedirect.com/science/article/pii/S1568494615000277. doi:https://doi.org/10.1016/j.asoc.2014.12.035.

[22] K. Hanbay, Deep neural network based approach for ECG classification using hybrid differential features and active learning, IET Signal Processing (2018). URL: https://digital-library.theiet.org/content/journals/10.1049/iet-spr.2018.5103. doi:10.1049/iet-spr.2018.5103.

[23] E. Deniz, Ann-based mppt algorithm for solar pmsm drive system fed by direct-connected pv array, Neural Computing and Applications 28 (2017) 3061–3072. URL: https://doi.org/10.1007/s00521-016-2326-4. doi:10.1007/s00521-016-2326-4.

[24] H. Guang-Bin, Z. Qin-Yu, S. Chee-Kheong, Extreme learning machine: a new learning scheme of feedforward neural networks, in: IEEE International Joint Conference on Neural Networks, volume 2, 2004, pp. 985–990. doi:10.1109/IJCNN.2004.1380068.

[25] O. A. Dobre, Y. Bar-Ness, Wei Su, Robust qam modulation classification algorithm using cyclic cumulants, in: 2004 IEEE Wireless Communications and Networking Conference (IEEE Cat. No.04TH8733), volume 2, 2004, pp. 745–748 Vol.2. doi:10.1109/WCNC.2004.1311279.

[26] H. Zamiri-Jafarian, S. Pasupathy, Adaptive state allocation algorithm in mlsd receiver for multipath fading channels: structure and strategy, IEEE Transactions on Vehicular Technology 48 (1999) 174–187. doi:10.1109/25.740085.

[27] D. Huang, C. Shan, M. Ardabilian, Y. Wang, L. Chen, Local Binary Patterns and Its Application to Facial Image Analysis: A Survey, IEEE Transactions on Systems Man and Cybernetics Part C-Applications and Reviews 41 (2011) 765–781. doi:10.1109/TSMCC.2011.2118750.

[28] G.-B. Huang, Q.-Y. Zhu, C.-K. Siew, Extreme learning machine: Theory and applications, Neurocomputing 70 (2006) 489 – 501. URL: http://www.sciencedirect.com/science/article/pii/S0925231206000385. doi:https://doi.org/10.1016/j.neucom.2005.12.126, neural Networks.

[29] Ö. F. Alçin, A. Şengür, M. C. İnce, Forward-Backward Pursuit Based Sparse Extreme Learning Machine, Journal of the Faculty of Engineering and Architecture of Gazi University Cilt 30 (2015) 111–117.

[30] G. F. Hepner, T. Logan, N. Pitter, N. Bryant, Artificial Neural Network Classification Using a Minimal Training Set : Comparison to Conventional Supervised Classification, Photogrammetric Engineering and Remote Sensing 56 (1989) 469–473.

[31] M. W. Aslam, Z. Zhu, A. K. Nandi, Automatic modulation classification using combination of genetic programming and

KNN, IEEE Transactions on Wireless Communications 11 (2012) 2742–2750. doi:10.1109/TWC.2012.060412.110460.
[32] O. Dobre, Y. Bar-Ness, Wei Su, Higher-order cyclic cumulants for high order modulation classification, in: IEEE Military Communications Conference (MILCOM), 2003, pp. 112–117. doi:10.1109/MILCOM.2003.1290087.
[33] V. Vijayarangan, R. Sukanesh, Reduction of peak to average power ratio in orthogonal frequency division multiplexing using pulse shaping techniques, International Journal of Electronics Engineering 1 (2009) 127–132.
[34] T. Dutta, U. Satija, B. Ramkumar, M. S. Manikandan, A novel method for automatic modulation classification under non-gaussian noise based on variational mode decomposition, in: 2016 Twenty Second National Conference on Communication (NCC), 2016, pp. 1–6. doi:10.1109/NCC.2016.7561103.
[35] S. Xi, H.-C. Wu, Robust Automatic Modulation Classification Using Cumulant Features in the Presence of Fading Channels, in: Wireless Communications and Networking Conference, 2006, pp. 2094–2099. doi:10.1109/WCNC.2006.1696619.
[36] O. A. Dobre, M. Oner, S. Rajan, R. Inkol, Cyclostationarity-based robust algorithms for qam signal identification, IEEE Communications Letters 16 (2012) 12–15. doi:10.1109/LCOMM.2011.112311.112006.

Table 2: Confusion matrix of the proposed classifier (%)

SNR = -2 dB	BPSK	QPSK	8-PSK	16-QAM	64-QAM	4-ASK
BPSK	100					
QPSK		94.5	5.5			
8-PSK		2.2	86.3	11.5		
16-QAM			9	90.9	0.1	
64-QAM				1.4	98.6	
4-ASK						100
SNR = 0 dB	BPSK	QPSK	8-PSK	16-QAM	64-QAM	4-ASK
BPSK	100					
QPSK		97.5	2.5			
8-PSK		0.5	93.4	6.1		
16-QAM			5	94.9	0.1	
64-QAM				0.8	99.2	
4-ASK						100

Table 3: Comparison of existing methods with proposed method

Feature-Classifier	Modulations	Channel	Setting	Accuracy (%)
Cumulants - Decision tree [4]	BPSK, QPSK, 8-PSK, 16-QAM	AWGN	N = 2048 SNR = 6 dB	95.5
LBP-ELM			N = 2048 SNR = 1 dB	97.4
Cumulants-GP/KNN [31]	BPSK, QPSK, 16-QAM, 64-QAM	AWGN	N = 2048 SNR = 7 dB	96
LBP-ELM			N = 2048 SNR = 0 dB	97
Normalized fourth-order cumulant - Decision tree [35]	QPSK, 16-QAM, 64-QAM	AWGN	N = 2048 SNR = 9 dB	94.2
LBP-ELM			N = 2048 SNR = -1 dB	96.1
Cyclostationarity - Optimum decision [36]	QPSK, 16-QAM, 64-QAM	AWGN $\Delta f/f_c = 0.03$ $\beta = 0.3$	N = 2048 SNR = 6 dB	96.6
LBP-ELM			N = 2048 SNR = 2 dB	97

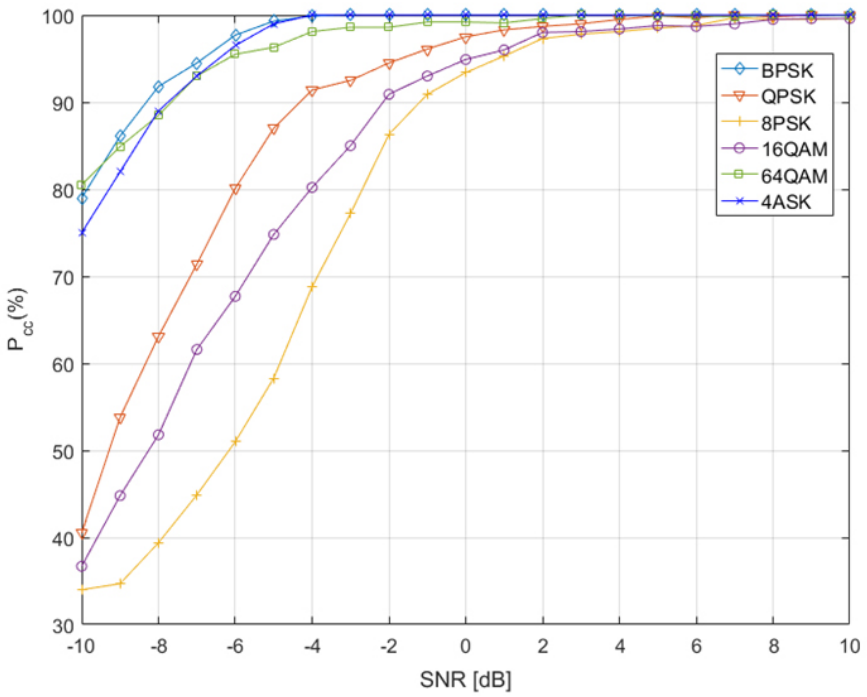

Figure 7: Classification accuracy of the proposed AMC classifier

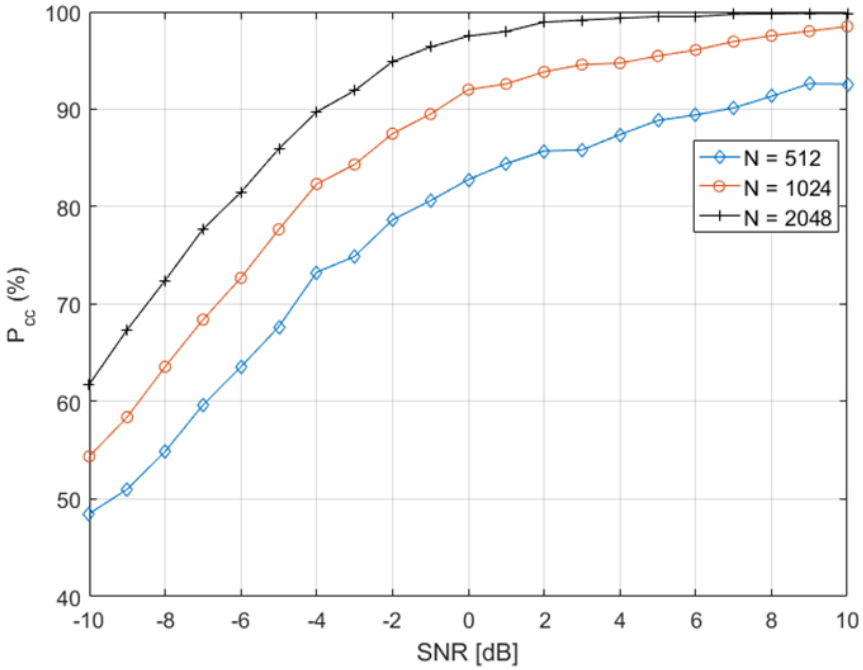

Figure 8: Average P_{cc} versus SNR for different number of symbols (N)

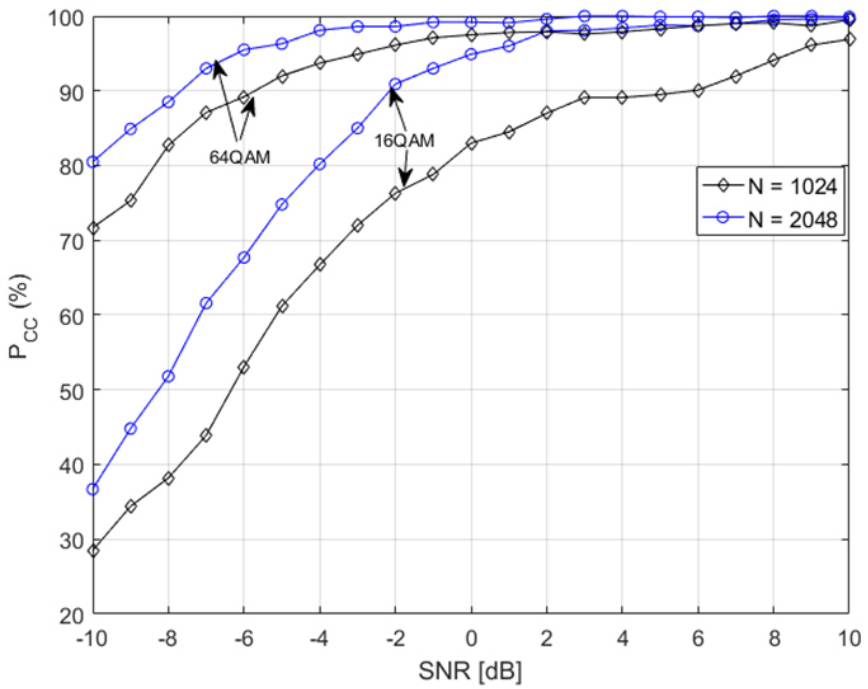

Figure 9: Performance of the proposed algorithm pertaining to the classification of MQAM modulations for different number of symbols (N)

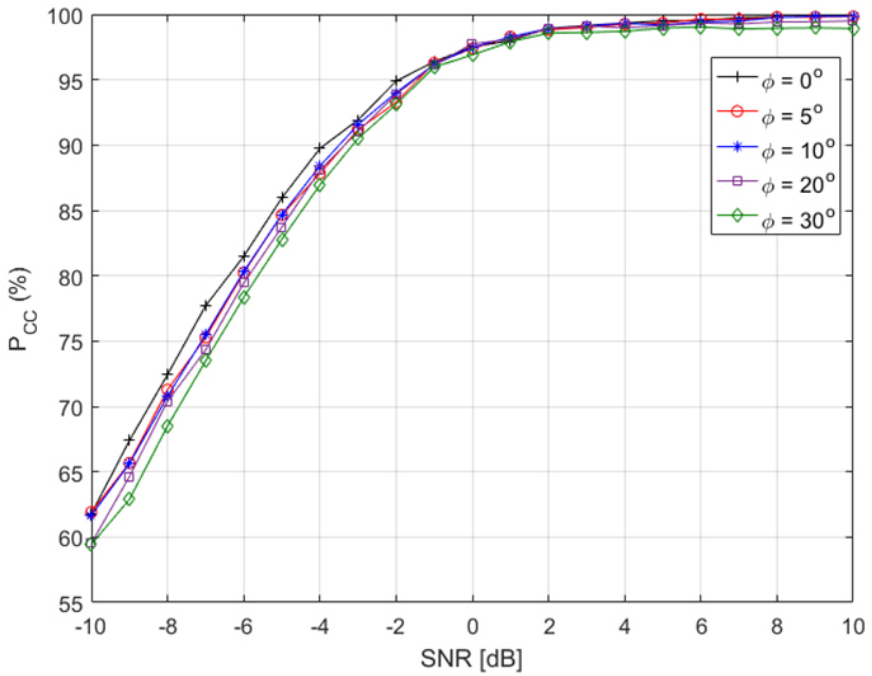

Figure 10: Average P_{cc} versus SNR for different values of phase offset (ϕ)

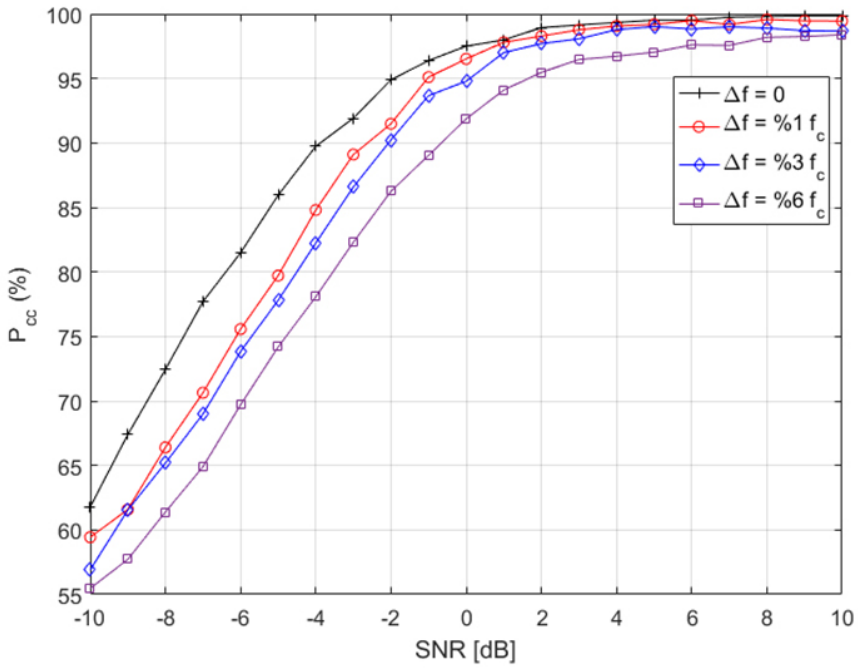

Figure 11: Average P_{cc} versus SNR for different values of frequency offset (Δf)

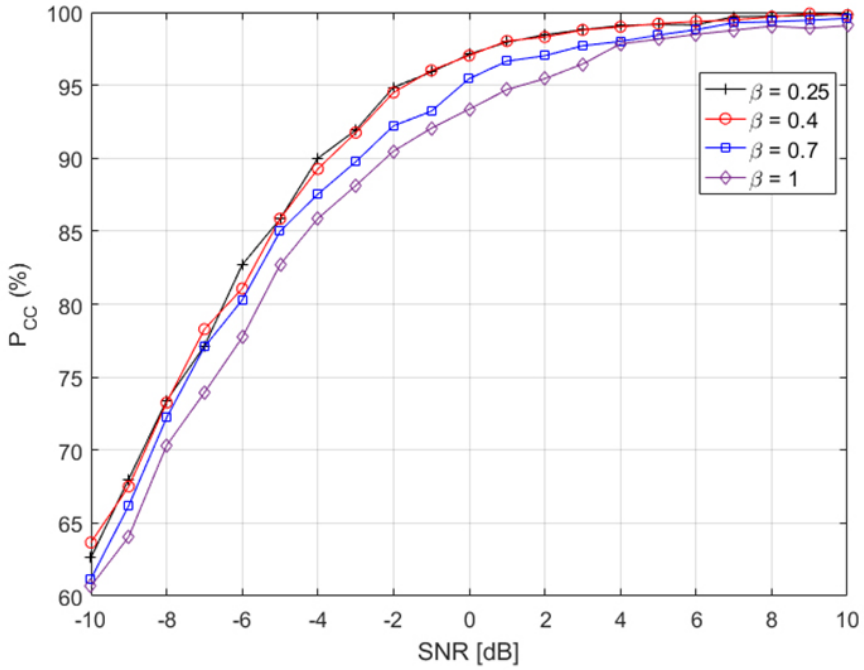

Figure 12: Average P_{cc} versus SNR for different values of roll-off factor (β)

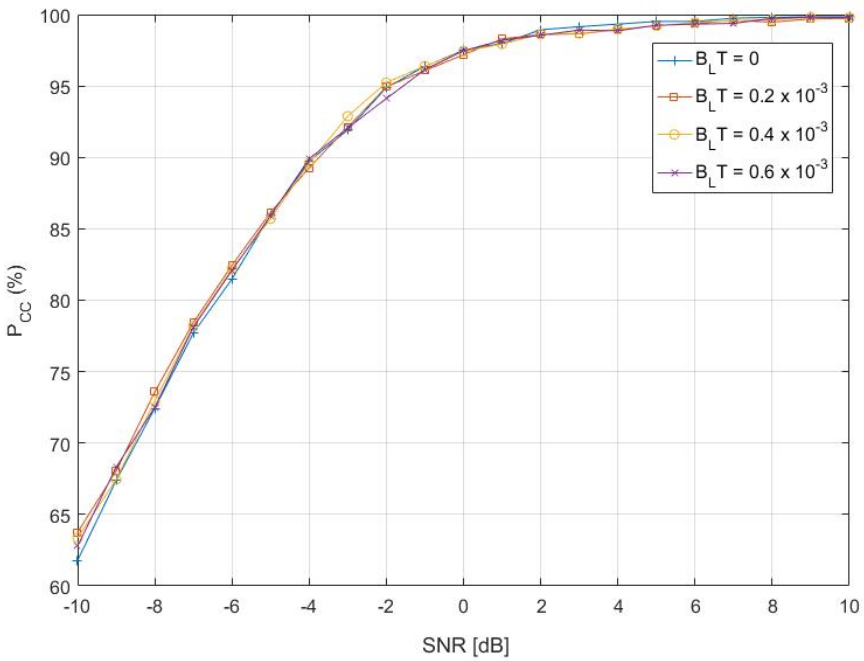

Figure 13: Average P_{cc} versus SNR for different values of phase noise bandwidth (B_L)

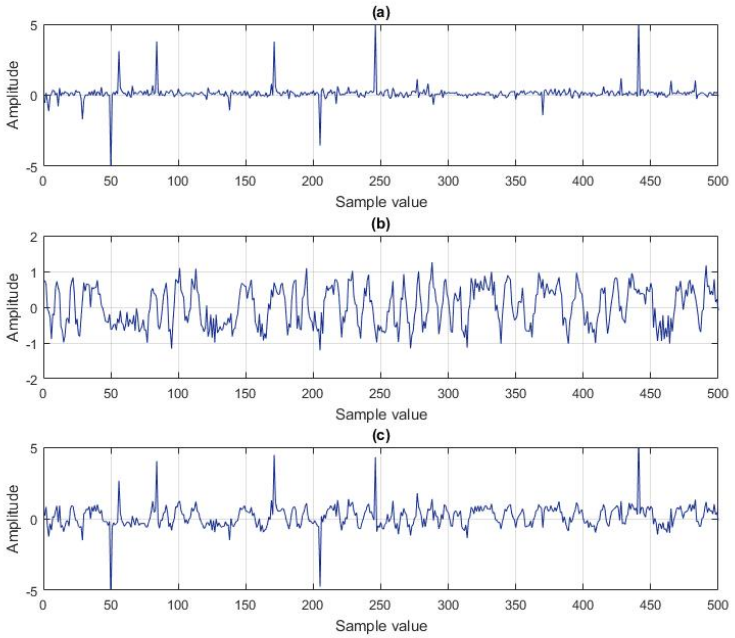

Figure 14: Digitally modulated signal with AWGN and impulsive noise. (a) impulsive noise with 10% random-valued impulse, (b) digitally modulated signal + AWGN with SNR = 10 dB, (c) digitally modulated signal + impulsive noise + AWGN with SNR = 10 dB

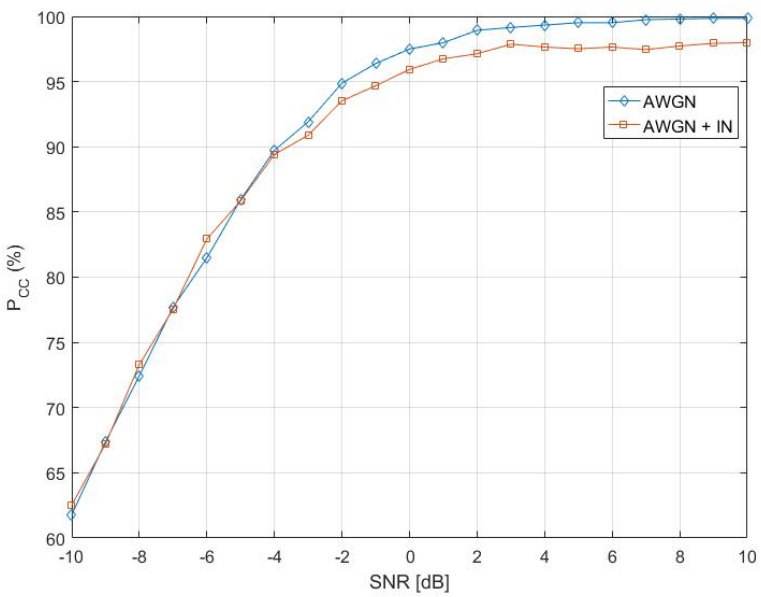

Figure 15: Average P_{cc} versus SNR in presence of AWGN and IN

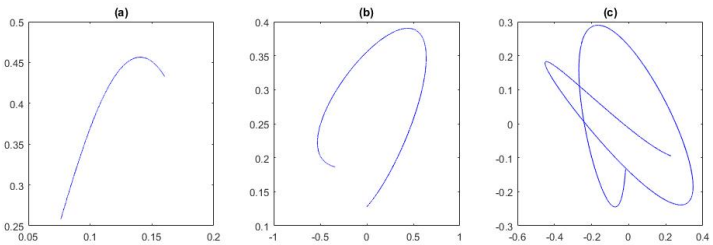

Figure 16: Change of channel coefficients with the effect of Doppler shift along the data packet for the signal with 3.5 GHz carrier frequency (a) $V = 10$ km/h (b) $V = 45$ km/h (c) $V = 90$ km/h

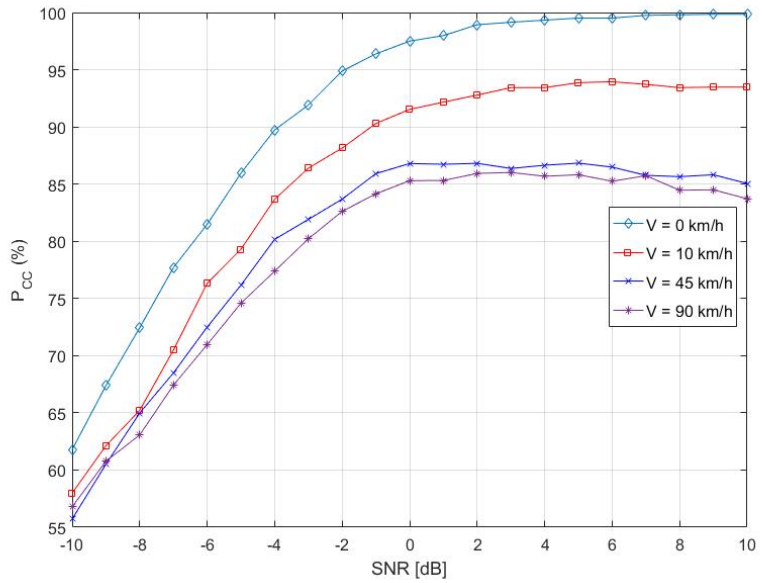

Figure 17: Average P_{cc} versus SNR for different values of velocity (V)

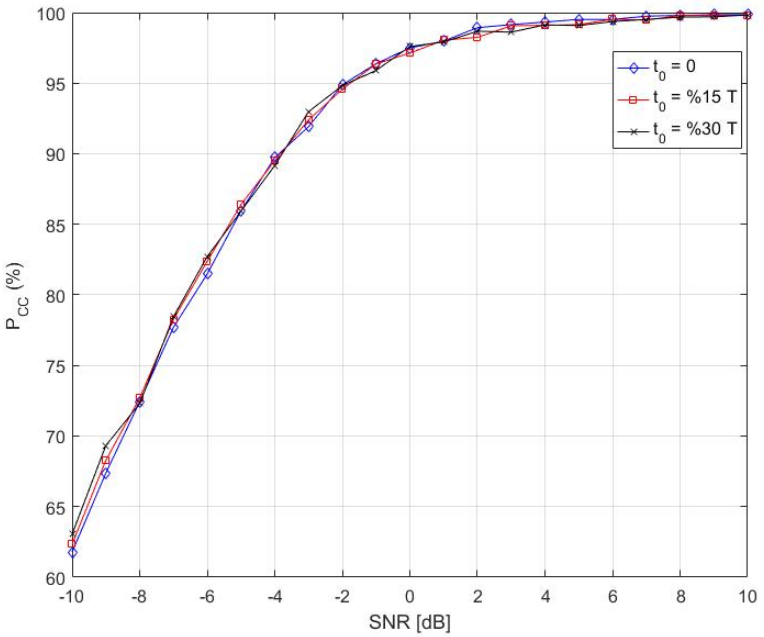

Figure 18: Average P_{cc} versus SNR for different values of timing offset (t_0)